Journal of Physics: Condensed Matter

OPEN ACCESS

RECEIVED
9 December 2025

REVISED
8 April 2026

ACCEPTED FOR PUBLICATION
27 April 2026

PUBLISHED
12 May 2026

PAPER

First-principles calculations of magnetic states in pyrochlores using a source-free exchange and correlation functional

Z Hawkhead[1], T L Breeze[1,*], N Gidopoulos[1], S J Blundell[2], S J Clark[1] and T Lancaster[1]

[1] Department of Physics, Centre for Materials Physics, Durham University, Durham DH1 3LE, United Kingdom
[2] Oxford University Department of Physics, Clarendon Laboratory, Parks Road, Oxford OX1 3PU, United Kingdom
* Author to whom any correspondence should be addressed.

E-mail: theodore.l.breeze@durham.ac.uk

Keywords: non-collinear magnetism, density functional theory, spin-ices

Supplementary material for this article is available online

Abstract

We present a first-principles investigation of the spin-ice state in $Dy_2Ti_2O_7$ using a magnetic source-free exchange and correlation (xc) functional, implemented in the CASTEP electronic-structure code. By comparing results from the conventional local spin-density approximation, we show that a spin-ice state in $Dy_2Ti_2O_7$ can be reliably obtained by removing the magnetic sources from the xc contributions to the potential, and we contrast this against the computed ground states of other frustrated pyrochlore magnets.

1. Introduction

Materials that show long-range, non-collinear magnetic spin textures occur widely in Nature [1–3]. A system with collinear order has a global quantisation axis along which all the spins are aligned or anti-aligned, while for a non-collinear state, each ordered spin can potentially have a different local direction. Such non-collinear states are commonly found, for example, in systems where the spin–orbit interaction leads, in a low-energy approximation, to single-ion anisotropy or to a Dzyaloshinskii–Moriya interaction [4–6].

Following the initial incorporation of collinear magnetism into density functional theory (DFT) within the local density approximation, attempts were made to describe non-collinear magnetism using the formalism of DFT. Studies of non-collinear magnetism appeared a decade after the introduction of spin-DFT [7], using disordered magnetic moments in the coherent-potential approximation [8–10] and with spin-spiral models [11–13]. Sandratskii and Guletskii obtained the band structure of a spin spiral in Fe without self-consistency [14] and in 1988 Kübler *et al* gave the first self-consistent band structure calculation of non-collinear magnetism [15]. For a review see [16, 17]. To incorporate spin–orbit coupling (SOC) required the development of a fully relativistic treatment [18]. To achieve this, all electrons are treated non-collinearly within the spin-polarised coupled Dirac equation. After development of the methods, the main hindrance in the use of DFT for non-collinear magnetism is the accuracy of the functionals. The optimised effective potential (OEP) method [19–21] has been shown [22] to successfully describe the magnitudes of magnetic moments, and therefore represents a candidate route to extend DFT's exchange and correlation (xc) functionals. Sharma *et al* [23] extended the spin-density formalism to non-collinear spin via the OEP, which has the advantage that it does not rely on the local collinearity of spins required when applying standard functionals. Eich and Gross [24] made a similar extension within a local density-like approximation.

Non-collinearity arises in a number of magnetic compounds that adopt the pyrochlore lattice, a three-dimensional arrangement of corner-sharing tetrahedra, which is known to exhibit a high degree of geometrical frustration [25, 26]. For example, the pyrochlore oxide $Dy_2Ti_2O_7$ [27] exhibits an interesting non-collinear magnetic structure owing to the strong Ising-like crystal-field anisotropy at each Dy site. The Dy^{3+} ions are magnetic and the $J = 15/2$ manifold is split by the crystal field, leading to a $\approx$10 μ_B ground state moment. The ground state is separated from crystal-field excited states by a gap

of a few hundred Kelvin [28]. The crystal-field anisotropy constrains the magnetic moments to lie along the local ⟨111⟩ axes [29, 30]. An effective ferromagnetic coupling between these moments results from the combination [31] of dominant long-range dipolar interactions ($D = 1.41$ K) with antiferromagnetic nearest-neighbour exchange ($J = -3.72$ K) [32]. As a result of this combination of interactions and the local anisotropy, below about 1 K the system settles into a disordered spin-ice state. This state is characterized by a '2-in 2-out' spin configuration (meaning that two spins point in and two spins point out of each tetrahedron), analogous to proton displacement vectors in Pauling's model of hydrogen disorder in water ice, the residual configurational entropy measured for these materials being close to Pauling's predicted value for ice [33, 34]. The excitations in spin ice are created by reversing a single spin, which thereby produces a pair of magnetic monopoles which can move independently through the lattice [35].

Studying these monopole excitations has become of great current interest [36–38], but an important scientific aim is to understand the local electronic properties of $Dy_2Ti_2O_7$ in more detail, particularly as the monopole transport may arise from the precise local arrangement of spins [38, 39]. Hitherto there have been limited first-principles simulations of the spin-ice state in $Dy_2Ti_2O_7$, and the spin-ice physics is generally understood within the low-energy description of the underlying magnetic energy-levels described above, invoking only crystal field levels and single-ion anisotropy effects [40, 41]. The bulk of the first-principles work carried out on pyrochlore materials focuses on electronic and structural effects. Early work investigating the electronic structure of a range of pyrochlores, including $Dy_2Ti_2O_7$, had success matching x-ray emission spectra [42]. Similar success has also been achieved in using DFT to study further pyrochlore materials [43, 44]. DFT has also been applied to compare the results of neutron scattering experiments in magnetic pyrochlores by calculating the phonon spectra [45]. Little work has been done from first-principles on the magnetic configurations of $Dy_2Ti_2O_7$, although there have been attempts at understanding magnetic behaviours in other magnetic pyrochlore materials [46–48].

Since the ordered spin-ice magnetic structure is inherently non-collinear and highly degenerate, it provides a challenge for spin-DFT calculations, particularly with the xc functionals currently at our disposal. Such systems result in large parameter spaces with complicated energy environments, which existing functionals fail to represent accurately owing to the inclusion of magnetic sources in the xc field [49]. As a result, minimisation into the correct magnetic ground state is not straightforward in these calculations. A question is whether DFT can stabilise the experimentally observed spin-ice state without imposing it through constraints or model Hamiltonians. In this work we show that removing magnetic source terms from the exchange-correlation allows the spin-ice configuration in $Dy_2Ti_2O_7$ to emerge within self-consistent spin-DFT, something that the local spin-density approximation (LSDA) fails to achieve. Here we present results of spin-DFT calculations where we make use of a source-free version of the well-known LSDA functional, which we have implemented into CASTEP, to stabilise the spin-ice state. By making comparisons to calculations performed using the conventional LSDA, we show that realising the spin ice state is possible because of the use of the source-free functional. We also present calculations on two further pyrochlore materials, $Nd_2Zr_2O_7$ and $Sm_2Ti_2O_7$, which are known to host an ordered *all-in, all-out* (AIAO) spin texture [50–52]. These latter examples show that the source-free LSDA correctly predicts that the AIAO state is of lower energy than a spin-ice state, which is not stable in the two materials considered. We anticipate that this new functional will prove useful in the study of other frustrated and non-collinear magnetic materials using DFT.

2. Source-free methods

2.1. Theory

The description of magnetism in electronic structure calculations uses the spin density, or equivalently, the magnetisation, which is a continuous vector field; computationally this is discretised onto a grid in order to perform calculations. For calculations of magnetic properties there are then two key parameters: the charge density $n(\boldsymbol{r})$ and the magnetisation density $\boldsymbol{m}(\boldsymbol{r})$. The accuracy of a DFT calculation depends on the choice of xc functional [53, 54], with different functionals capturing different aspects of a physical system. In standard DFT we have an xc functional $E_{\mathrm{xc}}[n]$ and an associated xc-potential, $V_{\mathrm{xc}}(\boldsymbol{r})$, given by the functional derivative:

$$V_{\mathrm{xc}}(\boldsymbol{r}) = \frac{\delta E_{\mathrm{xc}}[n(\boldsymbol{r})]}{\delta n(\boldsymbol{r})}. \tag{1}$$

In calculating the xc spin-potential for a non-collinear density we cannot use the analogue of equation (1), since the density in a non-collinear treatment is not a scalar field. Instead the electron

potentials can be expressed as 2×2 matrices, where we use spinors to account for the vector magnetisation [55]. We can express the xc spin potential in terms of a non-spin potential and a magnetic field via a four-component potential [55–57]

$$\mathcal{V}_{\mathrm{xc}}(\boldsymbol{r}) = V_{\mathrm{xc}}(\boldsymbol{r})\,\mathrm{I}_2 + \mu_{\mathrm{B}}\boldsymbol{B}_{\mathrm{xc}}(\boldsymbol{r}) \cdot \boldsymbol{\sigma}, \tag{2}$$

where the magnetic field $\boldsymbol{B}_{\mathrm{xc}}$ is the vector part of the xc potential, $\boldsymbol{\sigma}$ is the vector of Pauli spin matrices, μ_{B} is the Bohr magneton, and I_2 is the 2×2 identity matrix. We can then relate each term in equation (2) separately to E_{xc}: (i) the scalar potential $V_{\mathrm{xc}}(\boldsymbol{r})$ is found using equation (1), taking the density to be the scalar part of the non-collinear density; (ii) the vector term, or the magnetic field, is given by

$$\boldsymbol{B}_{\mathrm{xc}}(\boldsymbol{r}) = -\frac{\delta E_{\mathrm{xc}}[n(\boldsymbol{r}), \boldsymbol{m}(\boldsymbol{r})]}{\delta \boldsymbol{m}(\boldsymbol{r})}. \tag{3}$$

Much research has gone into developing xc functionals specific to non-collinear spin [23, 24]. However, there is no widely-used, accurate functional that consistently replicates experimentally-observed magnetic states, and most currently available xc functionals are simple extensions to functionals designed for collinear systems [58, 59]. To make use of functionals such as the LSDA, at each point in space we rotate the vector spin-density such that it lies along the z-axis, allowing us to decompose it into spin-up ($n_\uparrow$) and spin-down ($n_\downarrow$) densities which can be used to calculate E_{xc} [60, 61]. We then take the functional derivative of $E_{\mathrm{xc}}[n_\uparrow, n_\downarrow]$ with respect to $n_\uparrow$ and $n_\downarrow$. This yields $\boldsymbol{B}_{\mathrm{xc}}$ along the z-axis. Then, we carry out the inverse rotation on $\boldsymbol{B}_{\mathrm{xc}}$ and we finally obtain a non-collinear vector $\boldsymbol{B}_{\mathrm{xc}}$, which however remains locally parallel (at every point in real space) to the magnetisation density, or the spin density. As the resulting energy is calculated point-wise, the method imposes a non-physical constraint that the magnetisation must be locally collinear with $\boldsymbol{B}_{\mathrm{xc}}(\boldsymbol{r})$.

The authors of [56] highlight another important problem with standard functionals. From the Maxwell equations, for any arbitrary magnetic field, $\boldsymbol{B}$, the divergence of the field should be zero ($\boldsymbol{\nabla} \cdot \boldsymbol{B} = 0$), which follows from the absence of magnetic sources. However, this condition is not met for the common functionals, LSDA and PBE, which give results consistent with magnetic sources existing on the surfaces of a sample of the material. In [56] a method is suggested for improving these functionals that we reproduce in outline here. Starting from the Helmholtz theorem, a vector field can be decomposed into two components: one of which is divergence free and one that is curl free [62],

$$\boldsymbol{B}(\boldsymbol{r}) = \boldsymbol{\nabla} \times \boldsymbol{A} + \boldsymbol{\nabla}\phi. \tag{4}$$

To ensure that the magnetic field is source free we must explicitly subtract the term $\boldsymbol{\nabla}\phi$ that contributes to the divergence of the field. We have the freedom to select the gauge and chose ϕ such that it is the solution to the Poisson equation,

$$\nabla^2\phi(\boldsymbol{r}) = -4\pi\boldsymbol{\nabla} \cdot \boldsymbol{B}. \tag{5}$$

The source-free magnetic field $\tilde{\boldsymbol{B}}$ can then be constructed using

$$\tilde{\boldsymbol{B}}(\boldsymbol{r}) \equiv \boldsymbol{B}(\boldsymbol{r}) + \frac{1}{4\pi}\nabla\phi(\boldsymbol{r}), \tag{6}$$

and we can then obtain the xc magnetic field in terms of the substitution,

$$\boldsymbol{B}(\boldsymbol{r}) \to s\tilde{\boldsymbol{B}}(\boldsymbol{r}), \tag{7}$$

where s is an empirical scaling parameter.

We have implemented this source-free method in the plane-wave pseudopotential code CASTEP as a new xc functional labelled LDA_SF, which may be selected as a parameter when initialising a calculation. The source-free LSDA described in [56] is an alteration of the existing functional that requires only a manipulation of the xc magnetic field already present in LSDA calculations. Each time the xc energy and potential is calculated, the potential is used to construct the xc magnetic field $\boldsymbol{B}_{\mathrm{xc}}(\boldsymbol{r})$. Using the procedure described above, we can then calculate the source-free field $\tilde{\boldsymbol{B}}_{\mathrm{xc}}(\boldsymbol{r})$ and reconstruct the spin-potential. It is this potential that is then used in the Hamiltonian of the system. Critically, this is not a one-shot approach: the correction is calculated every time the xc potential is required and is therefore self-consistent.

To implement the method, we make use of the plane-wave basis set in order to efficiently solve the Poisson equation in equation (5). In a plane-wave basis, $\phi(\boldsymbol{r})$ can be expressed as

$$\phi(\boldsymbol{r}) = \sum_{\boldsymbol{G}_j} c_{\boldsymbol{G}_j} \mathrm{e}^{\mathrm{i}\boldsymbol{G}_j \cdot \boldsymbol{r}}, \tag{8}$$

where $\boldsymbol{G}_j$ are the reciprocal lattice vectors and $c_{\boldsymbol{G}_j}$ are the Fourier expansion coefficients of $\phi(\boldsymbol{r})$. The Fourier expansion allows us to efficiently compute the Laplacian of the scalar potential ϕ,

$$\nabla^2 \phi(\boldsymbol{r}) = -\sum_{\boldsymbol{G}_j} |\boldsymbol{G}_j|^2 c_{\boldsymbol{G}_j} \mathrm{e}^{\mathrm{i}\boldsymbol{G}_j \cdot \boldsymbol{r}}. \tag{9}$$

We can also express $\boldsymbol{B}_{\mathrm{xc}}(\boldsymbol{r})$ in terms of its Fourier coefficients $\boldsymbol{b}_{\boldsymbol{G}_j}$:

$$\boldsymbol{B}_{\mathrm{xc}}(\boldsymbol{r}) = \sum_{\boldsymbol{G}_j} \boldsymbol{b}_{\boldsymbol{G}_j} \mathrm{e}^{\mathrm{i}\boldsymbol{G}_j \cdot \boldsymbol{r}}. \tag{10}$$

For a given vector $\boldsymbol{G}_j$, the Fourier coefficients of $\boldsymbol{\nabla} \cdot \boldsymbol{B}_{\mathrm{xc}}(\boldsymbol{r})$ follow from

$$\mathscr{F}\left[\boldsymbol{\nabla} \cdot \boldsymbol{B}_{\mathrm{xc}}(\boldsymbol{r})\right](\boldsymbol{G}_j) = \mathrm{i}\boldsymbol{G}_j \cdot \boldsymbol{b}_{\boldsymbol{G}_j}, \tag{11}$$

where $\mathscr{F}$ denotes the Fourier transform. By rearranging equation (5) and substituting the reciprocal space expressions in equations (9) and (11), we come to an expression for the Fourier coefficients of $\phi(\boldsymbol{r})$,

$$c_{\boldsymbol{G}_j} = \frac{\mathrm{i}\boldsymbol{G}_j \cdot \boldsymbol{b}_{\boldsymbol{G}_j}}{4\pi |\boldsymbol{G}_j|^2}. \tag{12}$$

Knowing these coefficients, we can build the source-free magnetic field and reconstruct the spin-potential using equation (2). We note that the corrected xc potential is no longer strictly local as we use knowledge of the gradient of the potential when solving the Poisson equation. Owing to the use of a plane-wave basis set, these additional computations are very efficient; the source-free functional is still semi-local, and so results in calculations that are only slightly larger compared to the standard LSDA functional.

2.2. Tests on elemental magnetic materials

To test the validity of the implementation of the source-free LSDA, we performed calculations on a range of elemental magnets and magnetic compounds. The main focus of the testing is on body-centred cubic or α-Fe, where we performed magnetic calculations on a geometry optimised unit cell. Total energies are converged to better than 10 meV using a $7 \times 7 \times 7$ Monkhorst Pack (MP) $\boldsymbol{k}$-point-grid and a plane-wave cut-off radius of 1600 eV. We included SOC and used norm-conserving relativistic pseudopotentials throughout. Similarly, other calculations are converged to better than 100 meV/atom. Each of the materials tested have a ferromagnetic phase which we investigate using a quantisation axis aligned with the crystallographic c-direction. We initialised spin along this direction in each material to ensure that the energy minimisation returned a state with long-range magnetic order.

A useful way to assess the correction to $\boldsymbol{B}_{\mathrm{xc}}$ is to visualize the magnetic field lines, since it is easy to demonstrate that the source terms have been removed from the field.

In figure 1, we compare the field lines due to $\boldsymbol{B}_{\mathrm{xc}}$ in α-Fe. Using both the conventional LSDA (figures 1(a) and (b)) and the source-free LSDA (figures 1(c) and (d)) we find magnetic moments on each atom aligned along the c-axis. For the LSDA (figures 1(a) and (b)), the field lines are parallel throughout the entire infinite crystal, implying the presence of a magnetic source at the surface of the system. It is clear that these field lines for α-Fe are also globally collinear with the magnetisation, which is one of the issues with the LSDA highlighted in [56].

If instead we study the field lines due to the source-free functional (figures 1(c) and (d)) we see that they form closed loops around the Fe ions. As we have used the same quantisation axis in both calculation, the magnetisation is also collinear with the c-axis when using the source-free LSDA. However, it is clear then that the field lines for $\boldsymbol{B}_{\mathrm{xc}}$ are no longer constrained to be locally collinear with the magnetisation when the source terms are removed.

We see similar results for the $\boldsymbol{B}_{\mathrm{xc}}$ field lines in hexagonal close-packed (hcp) Co (figure 2). Using the LSDA (figure 2(a)) we again see parallel field lines aligning with the magnetisation which lies along the c-axis for both Co ions. From the source-free LSDA (figure 2(b)) we see the non-collinearity of the

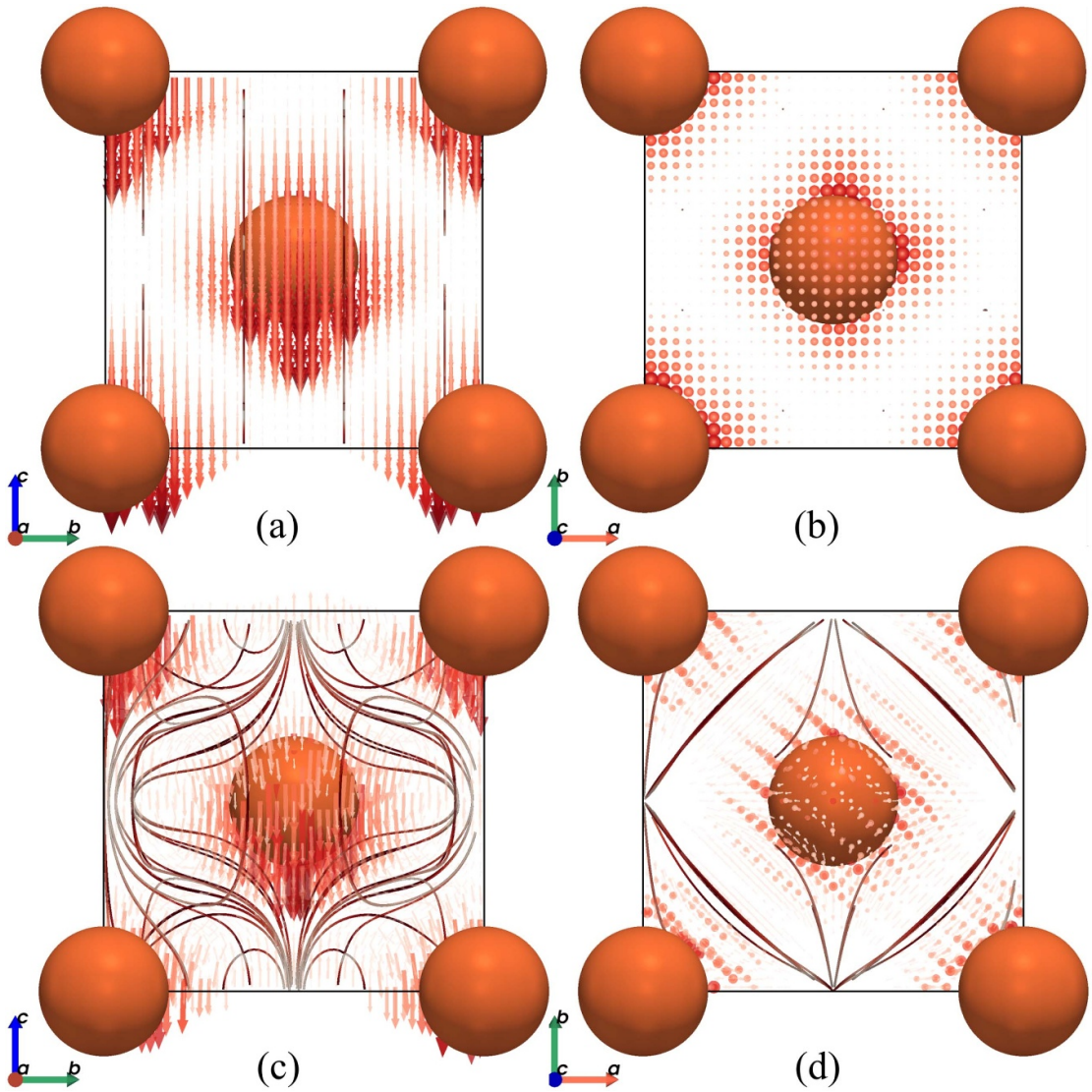

Figure 1. Field lines for $\mathbf{B}_{ex}$ in α-Fe calculated with the source-free and source-uncorrected LSDA. (a) and (b) xc field calculated using the conventional LSDA functional. (c) and (d) xc fields calculated using the source-free LSDA functional. Colour of the field lines represents the magnitude of the field at that point, from white at low fields to red at high fields. Vectors show the direction of the field flow with size and colour representing magnitude. These are plots of the discretised magnetisation from our basis grid. Where the field magnitude is lower than 10% of the maximum, vectors have been omitted for clarity. Magnetic moments lie in the negative *c*-direction in both cases.

field lines. Close to the Co ions, field lines emerge from the centre of the ion and terminate again at the centre of the ion. The behaviour further from the Co in the interstitial region is more complicated.

An example of the effects of the source-free functional on the xc field lines on a non-elemental magnet, FeTe, is shown in the supplemental material [63]. In this case, the field lines flow between the layers of Fe ions past the Te ions. It is less obvious that the xc field lines in FeTe represent a source-free field. We lose the simplicity of the elemental magnets by including non-magnetic ions which complicate the exchange interactions. However, we still see the improved non-collinearity arising from the source-free functional.

3. Spin ice ground states

We now turn to the application of the source-free methodology to the problem of the spin-ice magnetic structures. In order to model a spin-ice state in $Dy_2Ti_2O_7$ we used a primitive unit cell including 22 atoms, with lattice parameters of 7.19 Å calculated by DFT structural relaxation [64].

The spin structure was calculated with a 5×5×5 MP ***k***-point-grid with a plane-wave cut-off of 840 eV using norm-conserving relativistic pseudopotentials such that the calculations are converged to

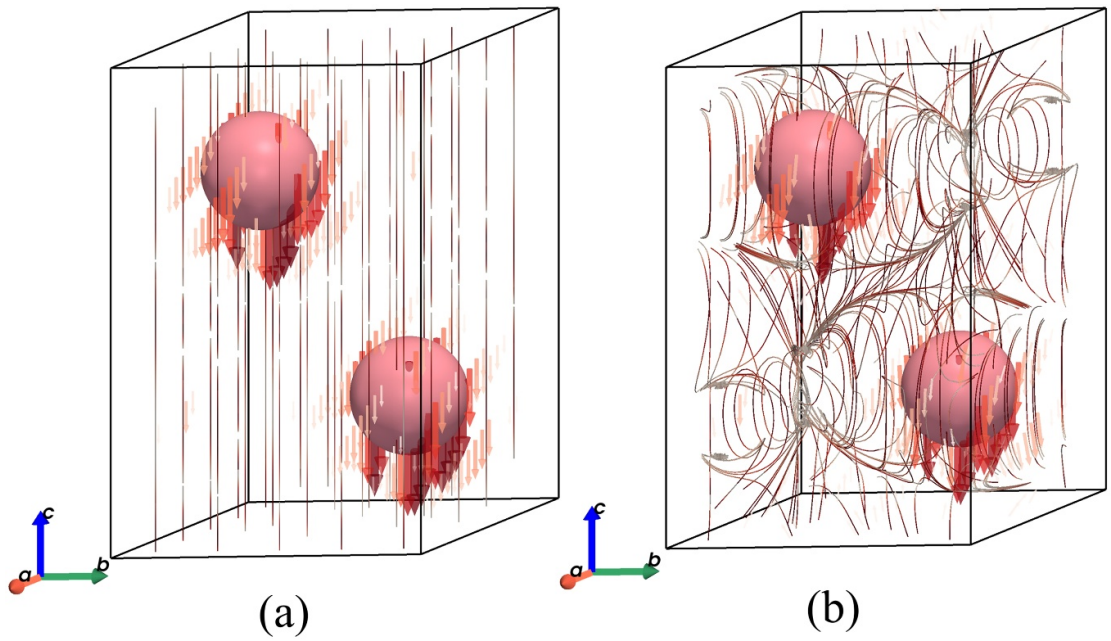

Figure 2. Magnetic field lines in hcp-Co calculated with (a) conventional LSDA and source-free LSDA. Colour of the field lines represents the magnitude of the field at that point, from white at low fields to red at high fields.

within 50 meV per atom. Convergence testing for $Dy_2Ti_2O_7$ is shown in the SM [63]. For calculations on $Nd_2Zr_2O_7$ and $Sm_2Ti_2O_7$ we used plane-wave cut-off energies of 843 eV and 860 eV respectively with a 5×5×5 MP $\boldsymbol{k}$-point-grid. The SCF calculation was performed using the ensemble density functional theory minimisation scheme. We performed identical calculations treating xc with both conventional LSDA and the newly-implemented source-free LSDA to compare the resulting spin configurations. In the case of both conventional LSDA and the source-free LSDA we initialise a non-collinear spin on each of the Dy ions along the direction of the local ⟨111⟩ direction in the 2-in-2-out spin ice configuration. Based on testing of the scaling parameter s in the SM [63], we conclude that there is no *a priori* reason to use any value other than $s = 1$ in equation (7), although it may still be used as an empirical parameter to better capture the experimental magnetic moments. However, we note that using extreme values of s (s>1.5 or s<0.5) can result in unphysical electronic structure.

We first examine the magnetic field lines of $\boldsymbol{B}_{xc}$ in $Dy_2Ti_2O_7$. The xc field lines for both functionals are shown in figure 3, where it is still possible to see that these remain locally collinear around the Dy ions in the case of the conventional LSDA (figure 3(a)), aligning with the magnetisation which is localised around these ions. In the interatomic regions it is less clear that the field lines are collinear, largely due to the lack of significant spin density. Instead these regions are dominated by numerical noise. However, for the source-free functional (figure 3(b)), the field lines display more obvious non-collinearity and no longer follow the magnetisation. We show below that by better capturing the physics of the internal fields using the source-free LSDA, we are able to realise the observed ground-state magnetic structure.

The improvement in non-collinearity provided by the source-free LSDA leads us to realise a spin-ice structure in $Dy_2Ti_2O_7$ which we find is not possible using conventional LSDA, despite using the same spin-ice initialisation. The resulting spin structures are shown in figure 4 where we have taken our spin density and projected it onto the Dy ions using Mulliken analysis. Calculations using non-collinear spins may fall into different local minima depending on the initialisation of the spin texture. In order to test the robustness of our method, these calculations were performed a number of times for different arrangements of spins conforming to the 2-in-2-out initialisation, and in each case for the given convergence parameters, we realise a spin-ice state using the source-free LSDA functional. Conversely, while conventional LSDA results in a non-collinear configuration of spins, there is no well-defined magnetic structure and a different arrangement is found each time (e.g. figure 4(a)), indicative of the randomly-initialised orbitals falling into a different local minimum each time we perform the calculation. By removing the unphysical source terms from the $\boldsymbol{B}_{xc}$ it appears we improve the energy landscape which

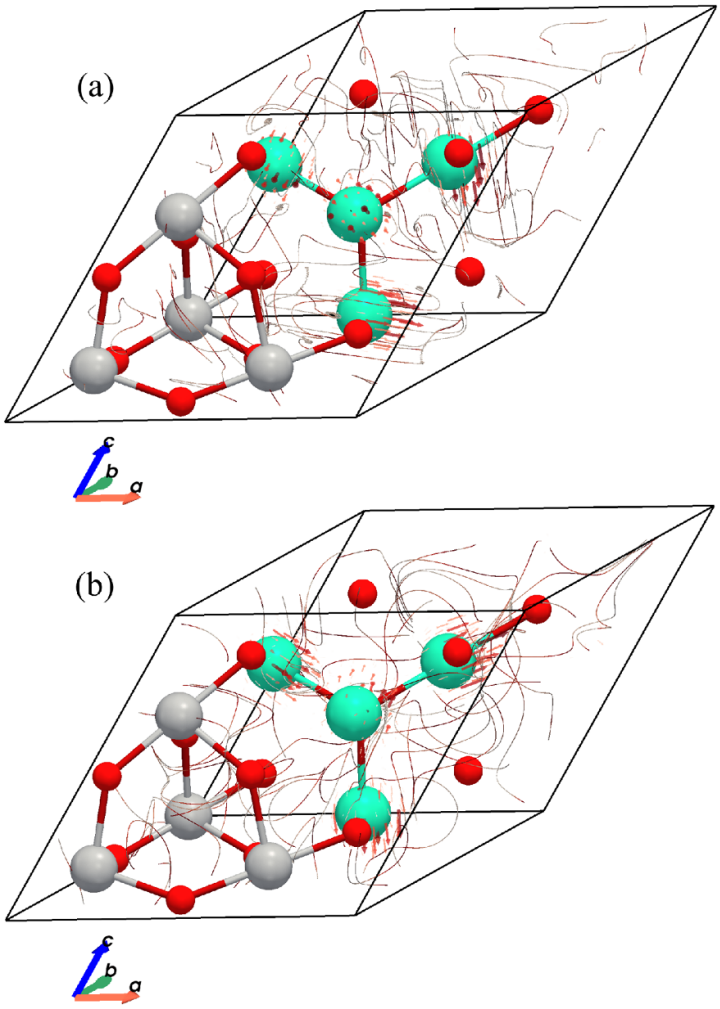

Figure 3. Magnetic field lines of $\mathbf{B}_{xc}$ for a primitive unit cell of $Dy_2Ti_2O_7$ calculated using the (a) conventional LSDA and (b) source-free LSDA, The opacity of the field lines represents the relative strength of the field. For the conventional LSDA field there is a local collinearity with the spin projected onto the Dy atoms, whereas for the source free functional B_{xc} is no longer aligned with the magnetisation. Dy, Ti and O ions are shown in green, silver and red respectively.

aids in the minimisation, and the source-free functional is then able to reliably reproduce the spin-ice structure in $Dy_2Ti_2O_7$ (figure 4(b)).

The treatment of localized f states often involves the inclusion of Hubbard U [65–68], as LSDA is known not to capture the correlation effects in these systems. We note that elsewhere in the literature [68, 69] generalised gradient approximation (GGA)+U calculations of the electronic structure of $Dy_2Ti_2O_7$ suggest that the inclusion of a Hubbard U parameter is required to describe the splitting of the Dy 4f bands observed in experiment. With the inclusion of a Hubbard U parameter in our LSDA calculations using the source-free functional and the DFT+U scheme we observe very similar effects on the density of states to those seen using the standard LSDA (and more broadly those seen using the PBE functional, as discussed in [68]), namely a straightforward splitting of the Dy 4f bands around the Fermi energy, where we do not expect the addition of a Hubbard U to affect the occupancies of bands in the ground state. Our calculations with a Hubbard U on the Dy 4f electrons of up to 4.5 eV minimize to the spin-ice structure. It is notable that a shortcoming of our approach is that LDA+U treatments of 4f states, while being more localized than pure LDA, do not have a structure described by LS-coupling, which is a prerequisite of a realistic crystal-field description of 4f states. As a result, LDA-computed crystal-field splittings of 4f states are typically significantly larger than those consistent with experiment. This implies that although we are able to realize the observed magnetic structure in $Dy_2Ti_2O_7$ the underlying electronic structure is not expected to be identical with the effective model (described in the introduction) that assumes that the $2J+1$ degenerate states that belong to the lowest energy, are split by crystal field effects.

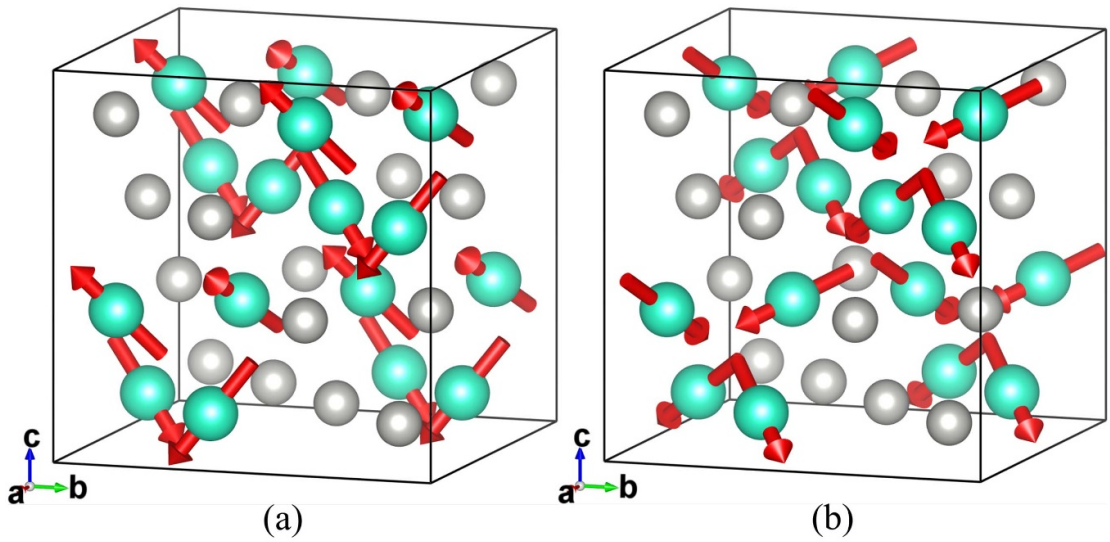

Figure 4. Example magnetic configurations of $Dy_2Ti_2O_7$ calculated using (a) conventional LSDA, and (b) source-free LSDA, shown in the conventional unit cell. Dy ions and Ti ions are shown in green and silver respectively. The red arrows show the non-collinear spin density projected onto a local atomic basis for the Dy ions. Oxygen atoms are not shown.

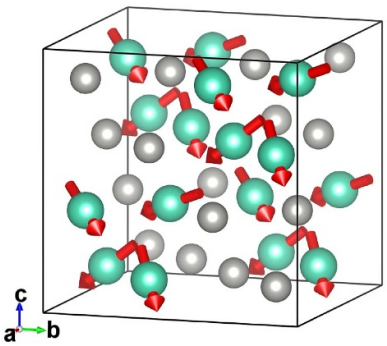

Figure 5. Example magnetic configurations of $Dy_2Ti_2O_7$ calculated using an all-in, all-out spin initialisation. Dy ions and Ti ions are shown in green and silver respectively. The red arrows show the non-collinear spin density projected onto a local atomic basis for the Dy ions. Oxygen atoms are not shown.

As was seen with the magnetic moment of our set of test materials (see supplemental material [63]), the spin-only magnetic moment on the Dy^{3+} is unchanged under the source-free functional, from $5.0\mu_B$ using conventional LSDA. The application of a Hubbard U parameter also does not significantly affect the moment size. This is in good agreement with experiment and with other DFT studies [69, 70].

To further test the capabilities of the source-free functional, we performed calculations on $Dy_2Ti_2O_7$ with the initial spin in both AIAO and random configurations. We see in figure 5 that the final spin orientation has not remained in the AIAO state, instead it has begun to fall into the spin-ice state seen above. Calculations with a random initialisation resulted in randomly oriented moments. Correspondingly, we find that the total energy of the spin-ice state in figure 4(b) is 2.2 eV lower in energy than the AIAO calculation and 0.85 eV lower than the randomly initialised calculations—well outside the computational uncertainty in both cases.

To show that the source-free functional provides systematic improvement to the magnetism in the wider class of materials, we have also performed calculations on $Nd_2Zr_2O_7$ and $Sm_2Ti_2O_7$ which are known to have an AIAO ground-state magnetic structure [50, 52, 71]. We initialised each calculation with both a spin-ice state and an AIAO state. In the case of $Nd_2Zr_2O_7$, the final spin configurations are shown in figure 6 (top). For the AIAO initialisation, we find that the resultant spin state is very similar to the initialisation, with some deviation from the local $\langle 111 \rangle$ direction. However, when we compare it to the result of a computation following initialisation in the spin-ice structure, which is known not to be a stable state in this material, we see a random arrangement of spins. This is much like the conventional LSDA calculations of $Dy_2Ti_2O_7$ shown in figure 4(a). The final AIAO state is found to be 0.4 eV lower in

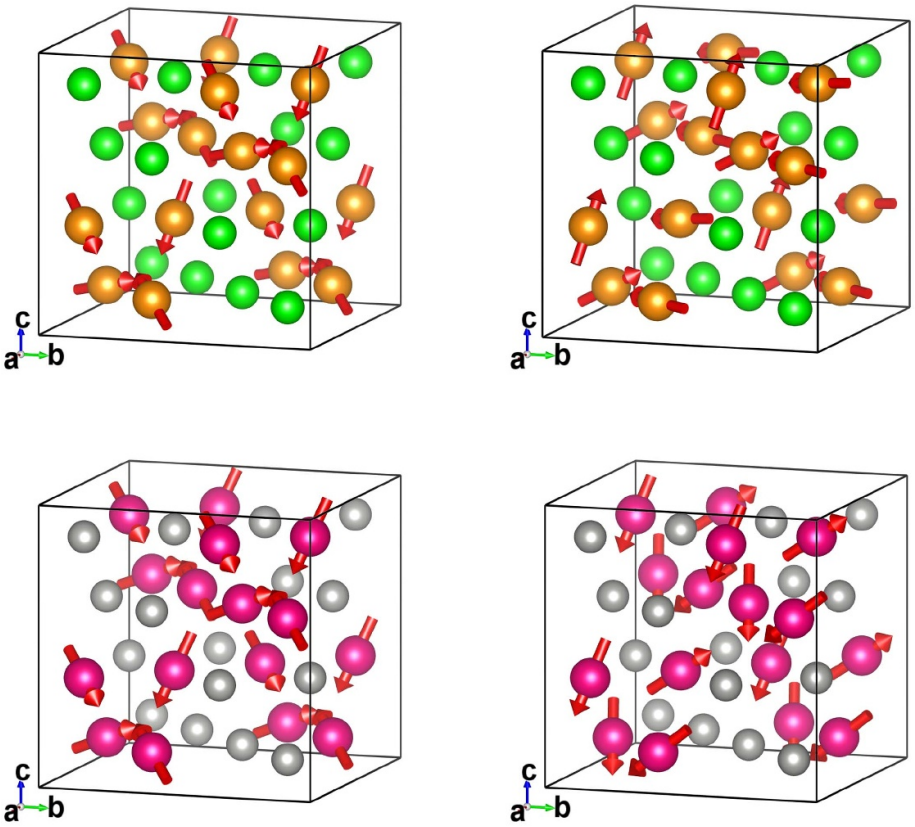

Figure 6. (Top) Example magnetic configurations of $Nd_2Zr_2O_7$ calculated using two different spin initialisations, (left) all-in, all-out and (right) spin-ice configurations. Nd ions and Zr ions are shown in orange and green respectively. The red arrows show the non-collinear spin density projected onto a local atomic basis for the Nd ions. (Bottom) Example magnetic configurations for $Sm_2Ti_2O_7$ calculated using two different spin initialisations, (left) all-in, all-out and (right) spin-ice configurations. Sm ions and Ti ions are shown in pink and silver respectively. Oxygen atoms are not shown.

energy than the state found by initialising a spin-ice. We see similar results for $Sm_2Ti_2O_7$ (figure 6 (bottom)) where we return an AIAO state and we fail to find a spin-ice configuration. In this latter case, the total energy for the AIAO state is found to be 1.0 eV lower that for state found following spin-ice initialisation. Interestingly, by initialising the spin-ice state in $Sm_2Ti_2O_7$, the final state is found to be similar to the ψ_2 ground state seen in a different pyrochlore, $Er_2Ti_2O_7$ [72–74].

4. Conclusions

In conclusion, we have implemented a recently-developed xc functional in a plane-wave code CASTEP, which provides a correction to the LSDA that removes magnetic sources from the resulting xc magnetic field, with the aim of improving the ability to describe non-collinear magnetic spin states. We have demonstrated our implementation of this functional by performing calculations on a number of simple magnetic materials. We applied the functional to the famous spin-ice material $Dy_2Ti_2O_7$ and find that where the LSDA is unable to capture the spin-ice state when initialised in this configuration, the source-free functional reproducible realises a spin-ice configuration. We are able to achieve these results using a method that is both simple to implement and is comparable to the LSDA in its computational expense. We hope that the availability of the source-free xc functional in CASTEP might allow the calculation of exotic magnetic textures which were previously inaccessible to DFT.

Acknowledgments

This work used the ARCHER UK National Supercomputing Service (https://www.archer.ac.uk) and is supported by EPSRC (UK) (EP/P022782/1). We are grateful for computational support from Durham Hamilton HPC. This work is supported by EPSRC (UK) [EP/N032128/1 and T.L.B's studentship].

Data availability statement

The data that support the findings of this study will be openly available following an embargo at the following URL/DOI: https://doi.org/10.15128/r18049g5150 [75].

Supplementary file available at https://doi.org/10.1088/1361-648X/ae6542/data1.

ORCID iDs

Z Hawkhead 0000-0001-6263-5237
T L Breeze 0009-0004-1939-2398
N Gidopoulos 0000-0002-0084-3548
S J Blundell 0000-0002-3426-0834
T Lancaster 0000-0002-6714-4215

References

[1] Bousquet E and Cano A 2016 *J. Phys.: Condens. Matter* **28** 123001
[2] Cheong S W and Huang F T 2024 *npj Quantum Mater.* **9** 13
[3] Rimmler B H, Pal B and Parkin S S 2025 *Nat. Rev. Mater.* **10** 109–27
[4] Weingart C, Spaldin N and Bousquet E 2012 *Phys. Rev. B* **86** 094413
[5] Vaidya S *et al* 2025 arXiv:2509.07173
[6] Lancaster T 2019 *Contemp. Phys.* **60** 246–61
[7] Von Barth U and Hedin L 1972 *J. Phys. C: Solid State Phys.* **5** 1629
[8] Oguchi T, Terakura K and Hamada N 1983 *J. Phys. F: Met. Phys.* **13** 145
[9] Hasegawa H 1979 *J. Phys. Soc. Jpn.* **46** 1504–14
[10] Gyorffy B, Pindor A, Staunton J, Stocks G and Winter H 1985 *J. Phys. F: Met. Phys.* **15** 1337
[11] You M and Heine V 1982 *J. Phys. F: Met. Phys.* **12** 177
[12] Haines E, Heine V and Ziegler A 1985 *J. Phys. F: Met. Phys.* **15** 661
[13] Sandratskii L M 1986 *Phys. Status Solidi b* **136** 167–80
[14] Sandratskii L and Guletskii P 1986 *J. Phys. F: Met. Phys.* **16** L43
[15] Kübler J, Höck K H, Sticht J and Williams A 1988 *J. Appl. Phys.* **63** 3482–6
[16] Kübler J 2009 Theory of itinerant electron magnetism *International Series of Monographs on Physics* (Oxford University Press)
[17] Sandratskii L 1998 *Adv. Phys.* **47** 91–160
[18] Yamagami H 2000 *Phys. Rev. B* **61** 6246
[19] Sharp R T and Horton G K 1953 *Phys. Rev.* **90** 317–317
[20] Talman J D and Shadwick W F 1976 *Phys. Rev. A* **14** 36–40
[21] Hollins T W, Clark S J, Refson K and Gidopoulos N I 2012 *Phys. Rev. B* **85** 235126
[22] Hollins T W, Clark S J, Refson K and Gidopoulos N I 2017 *J. Phys.: Condens. Matter* **29** 04LT01
[23] Sharma S, Dewhurst J K, Ambrosch-Draxl C, Kurth S, Helbig N, Pittalis S, Shallcross S, Nordström L and Gross E 2007 *Phys. Rev. Lett* **98** 196405
[24] Eich F and Gross E 2013 *Phys. Rev. Lett.* **111** 156401
[25] Trump B A *et al* 2018 *Nat. Commun.* **9** 2619
[26] Bramwell S and Harris M 1998 *J. Phys.: Condens. Matter* **10** L215–20
[27] Blöte H, Wielinga R and Huiskamp W 1969 *Physica* **43** 549–68
[28] Bertin A, Chapuis Y, de Réotier P D and Yaouanc A 2012 *J. Phys.: Condens. Matter* **24** 256003
[29] Harris M J, Bramwell S, McMorrow D, Zeiske T and Godfrey K 1997 *Phys. Rev. Lett.* **79** 2554
[30] Harris M J, Bramwell S T, Holdsworth P C W and Champion J D M 1998 *Phys. Rev. Lett.* **81** 4496–9
[31] den Hertog B C and Gingras M J P 2000 *Phys. Rev. Lett.* **84** 3430–3
[32] Castelnovo C, Moessner R and Sondhi S L 2011 *Phys. Rev. B* **84** 144435
[33] Ramirez A P, Hayashi A, Cava R J, Siddharthan R and Shastry B S 1999 *Nature* **399** 333–5
[34] Bramwell S T and Gingras M J 2001 *Science* **294** 1495–501
[35] Castelnovo C, Moessner R and Sondhi S L 2008 *Nature* **451** 42–45
[36] Morris D J P *et al* 2009 *Science* **326** 411–4
[37] Dusad R, Kirschner F K K, Hoke J C, Roberts B R, Eyal A, Flicker F, Luke G M, Blundell S J and Davis J C S 2019 *Nature* **571** 234–9
[38] Hallén J N, Grigera S A, Tennant D A, Castelnovo C and Moessner R 2022 *Science* **378** 1218–21
[39] Tomasello B, Castelnovo C, Moessner R and Quintanilla J 2019 *Phys. Rev. Lett.* **123** 067204
[40] Bramwell S T and Harris M J 2020 *J. Phys.: Condens. Mater.* **32** 374010
[41] Porée V *et al* 2022 *Phys. Rev. Mater.* **6** 044406
[42] Nemoshkalenko V, Borisenko S, Uvarov V, Yaresko A, Vakhney A, Senkevich A, Bondarenko T and Borisenko V 2001 *Phys. Rev. B* **63** 075106
[43] Hinojosa B B, Nino J C and Asthagiri A 2008 *Phys. Rev. B* **77** 104123
[44] Kang J, Fang Z, Chen X, Liu W, Guo F, Wu S, Zhang Y and Chen J 2014 *J. Alloys Compd.* **599** 170–4
[45] Ruminy M *et al* 2016 *Phys. Rev. B* **93** 214308
[46] Amirabbasi M and Alaei M 2020 *Phys. Rev. B* **102** 125105
[47] Huebsch M T, Nomura Y, Sakai S and Arita R 2022 *J. Phys.: Condens. Matter* **34** 194003
[48] Iqbal Y, Müller T, Riedl K, Reuther J, Rachel S, Valentí R, Gingras M J, Thomale R and Jeschke H O 2017 *Phys. Rev. Mater.* **1** 071201
[49] Krishna J, Singh N, Shallcross S, Dewhurst J, Gross E, Maitra T and Sharma S 2019 *Phys. Rev. B* **100** 081102

[50] Mauws C et al 2018 Phys. Rev. B 98 100401
[51] Bertin A et al 2015 Phys. Rev. B 92 144423
[52] Xu J, Anand V K, Bera A K, Frontzek M, Abernathy D L, Casati N, Siemensmeyer K and Lake B 2015 Phys. Rev. B 92 224430
[53] Lehtola S, Steigemann C, Oliveira M J and Marques M A 2018 SoftwareX 7 1–5
[54] Sousa S F, Fernandes P A and Ramos M J 2007 J. Phys. Chem. A 111 10439–52
[55] Gidopoulos N I 2007 Phys. Rev. B 75 134408
[56] Sharma S, Gross E, Sanna A and Dewhurst J 2018 J. Chem. Theory Comput. 14 1247–53
[57] Capelle K and Vignale G 2001 Phys. Rev. Lett. 86 5546
[58] Cuadrado R, Pruneda M, García A and Ordejón P 2018 J. Phys. Mater. 1 015010
[59] Pu Z, Li H, Zhang N, Jiang H, Gao Y, Xiao Y, Sun Q, Zhang Y and Shao S 2023 Phys. Rev. Res. 5 013036
[60] Kubler J, Hock K H, Sticht J and Williams A 1988 J. Phys. F 18 469
[61] Eschrig H and Pickett W 2001 Solid State Commun. 118 123–7
[62] Riley K F, Bence S J and Hobson M P 1997 Mathematical Methods for Physics and Engineering: a Comprehensive Guide (Cambridge University Press)
[63] Supplemental material contains a discussion of the parameter in eqn:forp, results of further tests on FeTe and further discussion of the energy minimization required to converge the computations.
[64] Persson K 2014 Materials data on $Dy_2Ti_2O_7$ (SG:227) by materials project
[65] Anisimov V I, Zaanen J and Andersen O K 1991 Phys. Rev. B 44 943
[66] Albers R, Christensen N E and Svane A 2009 J. Phys.: Condens. Matter 21 343201
[67] Wu H C, Lin S W and Wu J S 2012 J. Alloys Compd. 522 46–50
[68] Xiao H et al 2013 Adv. Condens. Matter Phys. 2013 675410
[69] Deilynazar N, Khorasani E, Alaei M and Hashemifar S J 2015 J. Magn. Magn. Mater. 393 127–31
[70] Gardner J S, Gingras M J and Greedan J E 2010 Rev. Mod. Phys. 82 53–107
[71] Lhotel E, Petit S, Guitteny S, Florea O, Hatnean M C, Colin C, Ressouche E, Lees M and Balakrishnan G 2015 Phys. Rev. Lett. 115 197202
[72] Lago J, Lancaster T, Blundell S, Bramwell S, Pratt F, Shirai M and Baines C 2005 J. Phys.: Condens. Matter 17 979
[73] McClarty P, Curnoe S and Gingras M 2009 J. Phys.: Conf. Ser. 145 012032
[74] de Réotier P D, Yaouanc A, Chapuis Y, Curnoe S, Grenier B, Ressouche E, Marin C, Lago J, Baines C and Giblin S 2012 Phys. Rev. B 86 104424
[75] Hawkhead Z, Breeze T L, Clark S J, Gidopoulos N, Blundell S J and Lancaster T 2026 First-principles calculations of magnetic states in pyrochlores using a source-free exchange and correlation functional (https://doi.org/10.15128/r18049g5150)